Nonquiescent Relaxation in Entangled Polymer Liquids after Step Shear

Shi-Qing Wang,* Sham Ravindranath, Pouyan Boukany, Michael Olechnowicz, Roderic P. Quirk, Adel Halasa,† and Jimmy Mays‡

Department of Polymer Science and Maurice Morton Institute of Polymer Science, University of Akron, Akron, Ohio 44325, USA

(Received 4 May 2006; published 2 November 2006)

Large step shear experiments revealed through particle tracking velocimetry that entangled polymeric liquids display either internal macroscopic movements upon shear cessation or rupturelike behavior during shear. Visible inhomogeneous motions were detected in five samples with the number of entanglements per chain ranging from 20 to 130 at amplitudes of step strain as low as 135%.

DOI: 10.1103/PhysRevLett.97.187801 PACS numbers: 61.25.Hq, 83.50.−v, 83.85.St

Many structured fluids share a universal characteristic known as viscoelasticity. These materials may be expected to behave like solids under external deformations. Specific microstructures determine the actual flow behavior of such complex systems as micelles, liquid crystals, polymers, colloids, foams, gels, glasses, granular materials, etc., As the microstructure rearranges in flow, the average rheological properties may exhibit nonlinear features such as strain softening, stress overshoot and shear thinning. For polymers, chain entanglement is a dynamic structure responsible for the observed sluggish relaxation dynamics. In quiescence, the entanglement is modeled with de Gennes's concept [1] of chain reptation in an impenetrable tube. The Doi-Edwards tube model [2] and its variations extended the notion of chain reptation and prescribed a scheme for depicting nonlinear flow behavior. It is widely recognized that the quantitative agreement [2] between the theoretical prediction [3–5] of the shear stress relaxation behavior upon large step strains and corresponding experimental observations [6] was an explicit validation of the Doi-Edwards tube theory and laid the foundation of the prevailing paradigm for polymer rheology [7].

However, another class of experimental data known as type C behavior [8–10] shows excessive strain softening and does not fit with this theoretical prediction of Doi and Edwards [2] and subsequent calculations based on a slip-link model [4]. A large body of literature has been devoted to an attempt to reconcile the apparent difference between experiment and theory. The original unphysical feature in the Doi-Edward tube model of a stress maximum for steady shear flow of entangled polymers [11] led subsequent workers [12–14] to speculate that the step shear deformation could occur inhomogeneously leading to the observed much lower relaxation modulus than that measured in the linear response regime. But no specific mechanism was put forward in these studies. The stress maximum character of the Doi-Edwards model has also been thought to be [15] the origin of the spurt phenomenon in capillary flow and to produce shear banding in steady simple shear flow [16]. However, over the past 20 years no shear banding has been seen for polymers and spurt has been shown to be only interfacial in nature. Subsequent studies on type C behavior led to studies of polymer slip [17,18] and secondary flow [18–20], where flow visualization in a step-strain experiment indicated ''delayed slip'' and visible movement of the sample near the shearing surfaces. Secondary flow was reported to occur near the edges in the plane-Couette shear because of the large meniscus. After two decades of investigation, the general consensus is that the type C behavior may be caused by polymer slip [21].

The present work only focuses on the "normal" type A relaxation behavior of entangled polymers. Our finding is that the phenomenon is far from expectation and not normal at all: instead of uniform quiescence after a step-strain, inhomogeneous macroscopic motion is observed throughout the sample thickness.

The Doi-Edwards tube theory made a famous prediction for the damping function [22], h, as shown in Fig. 1 for monodisperse entangled polymers; also plotted in Fig. 1 are the experimental data for a 10 wt% polybutadiene (PBD) solution (labeled as 0.74 M 10% below), made of a PBD from Bridgestone-America through courtesy of Dr. C. Robertson ($M_w = 738\,000$ and $M_n = 683\,000$ g/mol) dissolved in an oligomeric PBD (Sigma-Aldrich, catalog number 200433, $M_n \sim 1800$ g/mol). Measurements were taken with an Anton Paar MCR301 rotational rheometer coupled to a 25 mm cone-plate with a 2° cone angle. Indeed, agreement between the Doi-Edwards theory and our experimental data is reproduced in Fig. 1.

However, when expressing the actual stress, σ, at any long time [22], $t' > \tau_b$, as a function of the imposed strain, γ_0, surprising results were found as shown in the inset of Fig. 1. The normalized stress, $\sigma(t')/G_e(t') = \gamma_0 h(\gamma_0)$, shows a maximum at $\gamma_0 = 2.2$. If the chain entanglement network were to only suffer uniform deformation and to stay otherwise intact, we expect that the shear stress σ would only increase monotonically with γ_0. Thus, the inset in Fig. 1 forces us to ask the question of what the likely origin of the negative slope of σ vs γ_0 is.

We report here for the first time using a particle tracking velocimetric (PTV) technique described elsewhere [23] that entangled polymeric liquids do not remain quiescent after a large step shear. Equivalent results were found in

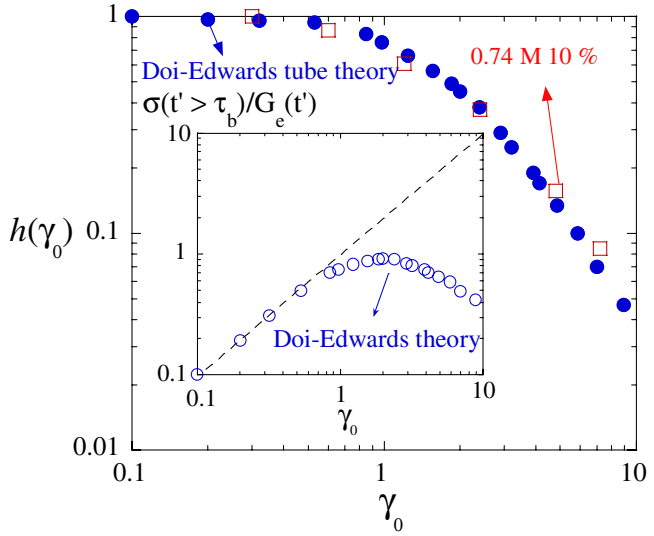

FIG. 1 (color online). The damping function obtained from large step-strain experiments on a 10% PBD solutions (0.74 M 10%) in open squares, along with the original theoretical prediction of the Doi-Edwards tube model in filled circles. The inset shows the shear stress vs the imposed strain γ_0 at times $t' > t_b$, which is derived directly from the damping function in the figure.

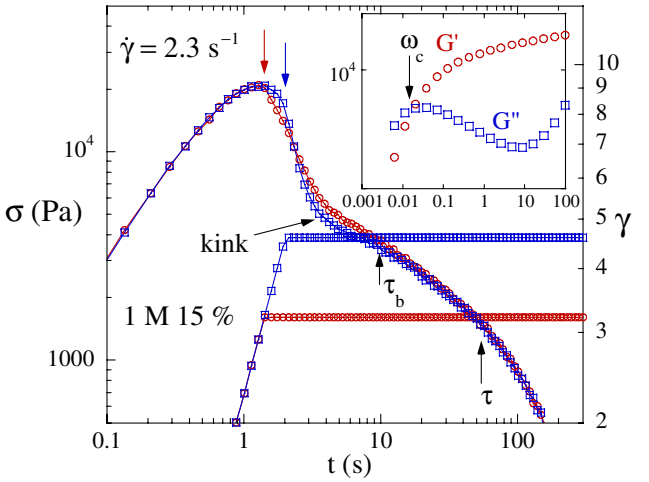

FIG. 2 (color online). Shear stress growth and relaxation behavior for two discrete step-strain experiments with $\gamma_0 = 3.2$ and 4.6, respectively, where the right Y axis shows the imposed averaged strain as a function of time. The inset shows the linear viscoelastic characteristics of the sample (1 M 15%).

both cone-plate and parallel-disk shear cells as well as in a home-made sliding-plate rheometer [24]. Below only some essential findings are presented and all other results will be deferred to future publications [24,25].

In this Letter, we report PTV observations on five entangled 1,4-polybutadiene (PBD) solutions with the number of entanglements per chain ranging from ca. 20 to 130: (1) 0.74 M 10%, which has been specified above; (2) 15 wt% PBD ($M_w = 1.8 \times 10^6$ and $M_n = 1.56 \times 10^6$ g/mol) dissolved in low MW PBD ($M_w = 3800$ and $M_n = 3500$), both made at Goodyear, labeled as 1.8 M 15%; (3) 15 wt% PBD ($M_w = 1.052 \times 10^6$ and $M_n = 1.014 \times 10^6$ g/mol) synthesized at Akron dissolved in a low MW PBD ($M_w = 8900$ and $M_n = 8500$ g/mol) made at Goodyear, labeled as 1 M 15%; (4) 4 wt% ultra high MW PBD ($M_w \sim 10^7$ g/mol, made at Akron) dissolved in the low MW PBD ($M_w = 8900$ and $M_n = 8500$ g/mol), labeled as 10 M 4%; (5) 5 wt% PBD ($M_w = 1.154 \times 10^6$, $M_n = 1.126 \times 10^6$, made at Tennessee) in the low MW PBD ($M_w = 8900$ and $M_n = 8500$ g/mol), labeled as 1.2 M 5%.

Figure 2 shows two discrete applications of step strain within 2 s on sample 3 (1 M 15%), in which there are 64 entanglements per chain. The inset shows that the sample possesses a terminal relaxation time of $\tau = 1/\omega_c = 56$ s. The two preset strains were achieved at the times indicated by the two arrows, respectively. For the lower step strain of $\gamma_0 = 3.2$, the shear stress was close to its maximum, whereas for the higher step strain of $\gamma_0 = 4.6$ the stress passed a maximum. In both cases, the stress declined rapidly during the first 8 s. Then a normal stress relaxation process ensued, leading to a good superposition. The time-strain separability is seen to occur after $t > \tau_b \sim 10$ s in these measurements. The kink in Fig. 2 has been seen numerous times in the past [6,13,17]. This type of measurement produces the information summarized in Fig. 1, where the decrease of the damping function, h, stems from the initial rapid stress decline.

We applied the recently developed PTV method [23] to visualize the step shear imposition and subsequent dynamic processes that have been thought to occur quiescently [26]. Using MGI Videowave 4 software, the analysis of the PTV observations shows that the sample experienced uniform deformation across H during shear for $\gamma_0 = 3.2$, as indicated in the inset of Fig. 3 by the linear velocity profiles at the beginning and at the end of shear. However, instead of any anticipated *quiescent* stress relaxation [26], significant movement of the sample was observed throughout its thickness after the step strain. The considerable macroscopic movement lasted about $\tau_b = 10$ s, during which the shear stress dropped sharply as shown in Fig. 2. This instability has been captured with a video camera and the video clip is available for online viewing [27]. As a simple way to characterize the behavior after a large step shear, we use vectors along the sample thickness to indicate the amounts of movement of the traced particles and their moving directions. As shown in Fig. 3, there are two special planes inside the sample where the nearby motions took place in opposite directions. The two arrows pointing to the original shearing direction near both boundaries of the sample indicate failure near the surfaces as well.

The visible movement of the traced particles, i.e., the macroscopic flow of the sample upon shear cessation can

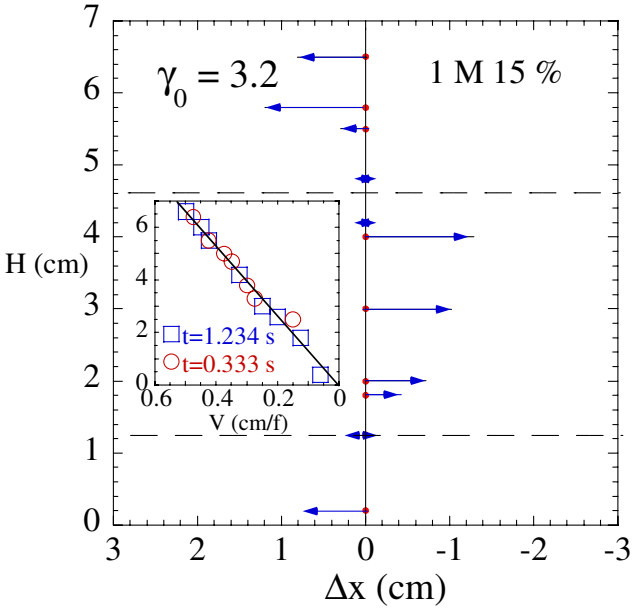

FIG. 3 (color online). The movement and direction of the traced particles upon completion of the prescribed strain described in Fig. 2, where the vectors show the particle displacements in each layer across the sample thickness, H, near the end of the unexpected macroscopic flow at $t \sim 8$ s (i.e., about 6.6 s after shear cessation) in the same units as determined by the computer screen for the gap distance, H. The shearing direction was to the left, thus $\Delta x > 0$ indicates the original flow direction and the red spots at $\Delta x = 0$ are the particle initial positions. An actual gap, H, of 0.9 mm shows up on the computer screen as ca. 7 cm in height. The inset indicates linear velocity profiles at two instants during the imposition of the large step strain of $\gamma_0 = 3.2$. The velocity is given in terms of the screen scale at a rate of 30 frames per second.

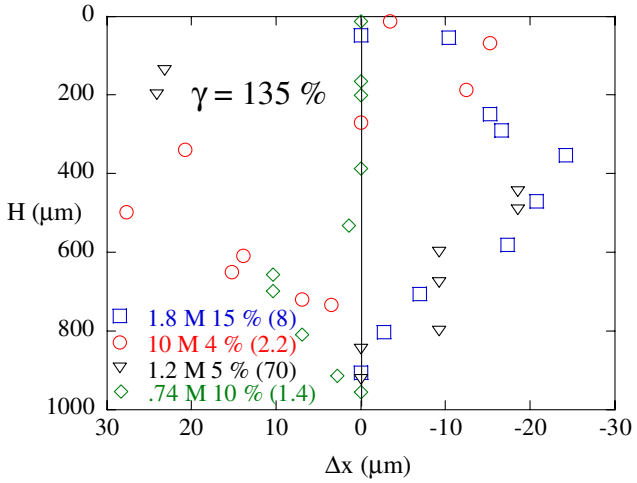

FIG. 4 (color online). The four samples (1.8 M 15%, 10 M 4%, 1.2 M 5%, and 0.74 M 10%) all experienced a step strain of ca. 135% at uniform shear rates 8, 2.2, 70, and 1.4 s^{-1}, respectively, as indicated in the parentheses of the labels. As in Fig. 3, $\Delta x = 0$ depicts the "equilibrium" position upon shear cessation. The four types of symbols indicate the locations of the traced particles in the different layers near the end of their macroscopic movements after the step strain, in each of the four step-strain experiments. Here the moving surface is the top plate situated at $H = 0$. The shearing direction was to the left; therefore, $\Delta x > 0$ represents particle motion in the original shearing direction, and $\Delta x < 0$ indicates particle movements in the opposite direction.

be seen for a step strain of amplitude just beyond $\gamma_0 = 1.0$, which is well below the values that cause the symptom of the stress maximum in Fig. 1. Figure 4 shows, for the four different samples, that macroscopic motions took place in various directions at a mere step strain of 135%. One video clip is available online [27] as Movie 7′ for the sample 1.8 M 15%.

There are several possible origins for the unexpected macroscopic motion after shear cessation. Backflow could take place if there was a residual shear stress gradient across the gap, analogous to capillary flow. However, the observed *linear* velocity profiles in the inset of Fig. 3 seem to exclude this explanation. Sample detachment or slip from the shearing surfaces could produce macroscopic movements near the surfaces as seen before [17], but both Figs. 3 and 4 show maximum movements in the interior away from the interfaces. Could the sample have broken up internally after suffering a large step strain? What force keeps the chain entangled? Because of lack of any existing notion, a tentative explanation is put forward here. Let us suppose that the visible motion after shear was due to internal disintegration through chain disentanglement. What would be the onset condition for such a process? A step strain of magnitude γ produces a shear stress $\sigma = G(\phi)\gamma$ in the linear region and would cause affine chain deformation, building an average elastic force $F_{\rm el}$ per chain given by $\nu(\phi)F_{\rm el} = G(\phi)\gamma$, where the chain surface density has the form of $\nu(\phi) \sim \phi\rho(N_a/M)R_0$ and the plateau modulus for a solution at weight fraction ϕ is $G(\phi) = G_N^0\phi[M_e/M_e(\phi)]$ in terms of the pure melt's plateau modulus $G_N^0 = 4\rho\kappa_B T N_a/5M_e$, with the entanglement molecular weight $M_e(\phi)$ related to the entanglement spacing $l_{\rm ent}$ as $l_{\rm ent}^2 \sim M_e(\phi)$. With increasing γ, the elastic force borne by each entangled chain would increase until the chain could afford an appreciable entropic loss from conformational distortion to free itself from the entangling medium. In order to undergo this entropically unfavorable transformation or rearrangement a force would need to be overcome that allows the wiggling chain to thread through a narrow opening that is plausibly comparable to the mesh size $l_{\rm ent}$. This entanglement force can be estimated to be given by $F_{\rm ent} \approx k_B T R_0/l_{\rm ent}^2$. By equating $F_{\rm ent}$ with $F_{\rm el}$, we find a critical condition of $\gamma_c \sim 5/4$, independent of the level of chain entanglement. This condition seems consistent with the behavior found in Fig. 4 where detectable macroscopic motion was seen in the various samples for a step strain merely above 5/4.

For a larger step strain of $\gamma_0 = 4.6$, the inset of Fig. 5 shows that the velocity profile was also linear (circles) in

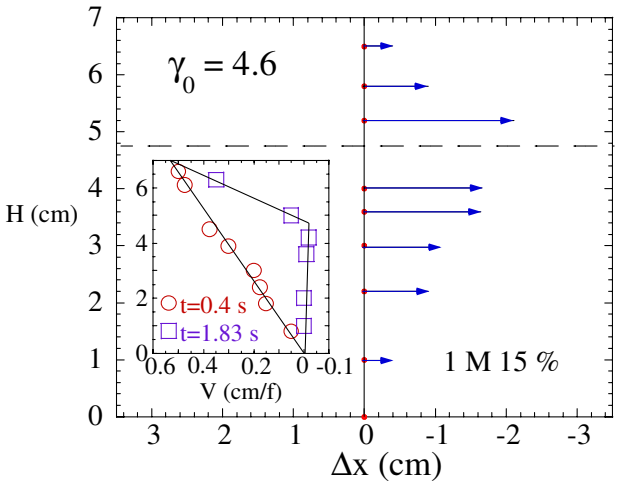

FIG. 5 (color online). An approximate quantification of the early motions of the traced particles 0.17 s after completion of the imposed strain in terms of their displacements, where the horizontal dashed line indicates the fault plane produced during shear. The inset shows the velocity profiles at two instants during the imposition of the large step strain of $\gamma_0 = 4.6$. The remarkable velocity profile at $t = 1.83$ s indicates rupturelike behavior during shear.

the initial stage of shearing. The velocity profile (in squares) in the inset of Fig. 5 appears to reveal rupturelike behavior as about $2/3$ of the entire sample adjusted from the linear profile (in circles) to that represented by the squares, and the measured shear stress dropped sharply as seen in Fig. 2. A similar PTV analysis of the macroscopic motion after shear cessation produces Fig. 5 where the vectors show the distribution of these traced particles across the sample thickness at a moment about 0.17 s after shear cessation.

In summary, the particle tracking velocimetric observations indicated macroscopic motion throughout the sample after application of a step strain instead of revealing a quiescent sample. Visible nonuniform motions were seen for four samples with different levels of chain entanglement at a mere step strain of 135%, which is a much lower amplitude than where the original Doi-Edwards tube theory indicated a stress maximum in Fig. 1. Thus, we have been compelled to put forward a new explanation of the observed phenomenon. Specifically, we speculated that as a sufficient elastic force builds up due to the imposed shear, a chain might overcome an entropic barrier (that normally prevents rapid conformational distortion in equilibrium) to assume, in a short time, a new conformation with much reduced entanglement interactions with the surrounding medium.

This work is supported, in part, by a Small Grant for Exploratory Research of the National Science Foundation (No. DMR-0603951) and an ACS grant No. (PRF #40596-AC7). SQW appreciated some helpful comments on the manuscript by Alan Gent.

*Email: swang@uakron.edu
†Goodyear Tire & Rubber Company-Research and Development, Akron, OH 44305, USA.
‡Department of Chemistry, University of TN, Knoxville, TN 37996, USA.

[1] P. G. de Gennes, J. Chem. Phys. **55**, 572 (1971).
[2] M. Doi and S. F. Edwards, *The Theory of Polymer Dynamics* (Clarendon Press, Oxford, 1986).
[3] M. Doi, J. Polym. Sci. **18**, 1005 (1980).
[4] M. Doi and J. Takimoto, Phil. Trans. R. Soc. A **361**, 641 (2003).
[5] R. S. Graham, A. E. Likhtman, T. C. B. McLeish, and S. T. Milner, J. Rheol. (N.Y.) **47**, 1171 (2003).
[6] K. Osaki, K. Nishizawa, and M. Kurata, Macromolecules **15**, 1068 (1982).
[7] W. W. Graessley, Adv. Polym. Sci. **47**, 67 (1982).
[8] K. Osaki, Rheol. Acta **32**, 429 (1993).
[9] K. Osaki and M. Kurata, Macromolecules **13**, 671 (1980).
[10] C. M. Vrentas and W. W. Graessley, J. Rheol. (N.Y.) **26**, 359 (1982).
[11] M. Doi and S. F. Edwards, J. Chem. Soc., Faraday Trans. 2 **75**, 38 (1979).
[12] G. Marrucci and N. Grizzuti, J. Rheol. (N.Y.) **27**, 433 (1983).
[13] R. G. Larson, S. A. Khan, and V. R. Raju, J. Rheol. (N.Y.) **32**, 145 (1988).
[14] F. Morrison and R. G. Larson, J. Polym. Sci., Part B: Polym. Phys. **30**, 943 (1992).
[15] T. C. B. McLeish and R. C. Ball, J. Polym. Sci., Polym. Phys. Ed. **24**, 1735 (1986).
[16] M. E. Cates, T. C. B. McLeish, and G. Marrucci, Europhys. Lett. **21**, 451 (1993).
[17] L. A. Archer and R. G. Larson, J. Rheol. (N.Y.) **39**, 519 (1995).
[18] L. A. Archer and R. G. Larson, J. Fluid Mech. **301**, 133 (1995).
[19] M. J. Reimers and J. M. Dealy, J. Rheol. (N.Y.) **40**, 167 (1996).
[20] V. R. Mhetar and L. A. Archer, J. Rheol. (N.Y.) **40**, 549 (1996).
[21] D. Venerus, J. Rheol. (N.Y.) **49**, 277 (2005). This paper provides an excellent review of the state-of-art understanding of the subject up to now.
[22] In the nonlinear response regime, a damping function, h, is traditionally introduced as a normalized relaxation modulus: $h(\gamma_0) = \sigma(t)/\gamma_0 G_e(t) \equiv G(t, \gamma_0)/G_e(t)$, for $t > \tau_b$, where G_e is the relaxation modulus in the linear response regime.
[23] P. Tapadia and S. Q. Wang, Phys. Rev. Lett. **96**, 016001 (2006); P. Tapadia, S. Ravindranath, and S. Q. Wang, Phys. Rev. Lett. **96**, 196001 (2006).
[24] P. Boukany *et al.* (to be published).
[25] S. Ravindranath *et al.* (to be published).
[26] The inertia is totally negligible, i.e., the sample would stop moving as soon as the top surface has come to a stop, within a time scale on the order of $\rho H^2/\eta < 10^{-6}$ s.
[27] Click Movie 6 at URL: http://www3.uakron.edu/rheology/ to view the video corresponding to the step-strain experiment ($\gamma_0 = 3.2$) described in Figs. 2 and 3.